Desalination and Water Treatment
www.deswater.com

doi:10.5004/dwt.2018.23028

131 (2018) 328–342
November

Congo red dye removal under the influence of rotating magnetic field by polypyrrole magnetic nanocomposite

Uyiosa Osagie Aigbe[a], Mohammed Khenfouch[a], Wei Hua Ho[b], Arjun Maity[c], Vijaya Srinivasu Vallabhapurapu[a], Nanjundaswamy Marishetty Hemmaragala[a,*]

[a]*Department of Physics, College of Science, Engineering and Technology, University of South Africa, Pretoria, South Africa, email: uyi4we@yahoo.co.uk (U.O. Aigbe), khenfouch@yahoo.fr (M. Khenfouch), vallavs@uisa.ac.za, vvsrinivasu@hotmail.com (V.S. Vallabhapurapu), nswamyorg@gmail.com, hemmanm@unisa.ac.za (N.M. Hemmaragala)*
[b]*Department of Mechanical and Industrial Engineering, College of Science, Engineering and Technology, University of South Africa, Pretoria, South Africa, email: howh@unisa.ac.za (W.H. Ho)*
[c]*DST/CSIR National Centre for Nano structured Materials, Council for Scientific and Industrial Research, Pretoria 0001, South Africa, email: AMaity@csir.co.za (A. Maity)*

Received 27 January 2018; Accepted 24 August 2018

ABSTRACT

Studies on magnetic field exposure of congo red contaminated water employing polypyrrole magnetic nanocomposite is reported. Alternating magnetic poles as a function of time has been used to move functionalized nanoparticles in congo red contaminated water. A maximum removal of 94% was observed for the adsorption of 100 mg/L of the adsorbate using 0.15 g of adsorbent at a magnetic field and exposure time of 18.99 mT and 120 min. Percentage of congo red dye removed increased with an increase in the magnetic exposure time of 10–120 min (79–94%). The magnetic force exerted on the magnetic nanoparticles leads to increased adsorption of congo red owing to increased velocity and reorientation of the charged particles. The Langmuir isotherm model had the highest correlation coefficient value and fitted well with the experimental data. The maximum adsorption capacity of 119.76 mg/g was observed using this isotherm model.

Keywords: Azo dyes; Congo red; Magnetic field; Nanocomposite; Water treatment

1. Introduction

Water is essential to every living being on earth and an important resource for human development. Unfortunately, civilization and industrialization affect the purity of water due to the pollution by toxic substances, heavy metals, pigments and dyes [1–3]. Synthetic dyes have become inevitable in modern life. Though azo dyes are known to be highly carcinogenic, their use has become part of human life which is a major threat for ecological concern as coloured wastes/effluents from manufacturing and fabric industries released to the environment [4–7]. An example of a benzidine-based anionic azo dye having complex aromatic structure is congo red (CR) dye. Since congo red dye wastes are hazardous, toxic, non-biodegradable and carcinogenic to human, special attention is given to remove these contaminants from the environment [8–11]. Removal of dyes from water has significant environmental, technical, and commercial importance and continuous efforts are going on to develop efficient and cost-effective removal methods. These techniques include adsorption of dye contaminants onto mineral or carbon-based matrices, photo-catalysis or oxidation processes, microbiological or enzymatic decomposition, etc. Among all available techniques, adsorption is regarded as more effective because of its simplicity and ease of operation [12–15].

On the other hand, owing to its broad spectrum of applications, the magnetic field (MF) finds importance

*Corresponding author.

in the fields such as therapeutic and diagnostic medicine, environmental management and industries over the years. Addressing environmental problems using magnetic technique has received substantial consideration in recent times [16–18]. Application of the magnetic field in water treatment has been known to be effective in numerous instances, due to their ecological purity, safety, and simplicity [19–21]. In continuation of our interest in exploring magnetic techniques for the treatment of contaminated water, herein we report the studies employing polypyrrole magnetic nanocomposite as an adsorbent to evaluate magnetic field effect created by modified three-phase induction motor for congo red dye adsorption. Other parameters like magnetic exposure time, pH, initial concentration and adsorbent dosage effects on congo red adsorption have also been evaluated. The goal is to create a water treatment technique, which would be useful for further application in the removal of congo red dye from wastewater effluents.

2. Experimental

2.1. Materials and methods

All chemicals were of analytic grade and used without further purification. Ferric chloride, magnetite (Fe_3O_4), pyrrole (Py), sodium hydroxide, hydrochloric acid and congo red dye was purchased from Sigma-Aldrich, South Africa.

2.2. Synthesis of adsorbent

In-situ chemical oxidative polymerization technique was used for the preparation of polymer-based magnetic nanocomposite (PPy/ Fe_3O_4) as described by [22]. 0.4 g of magnetite (Fe_3O_4) was added to the 80-mL deionized water in a 250 mL Erlenmeyer flask, which was sonicated for 30 min to have a proper distribution of the magnetite particles in the deionized water solution. Then, 0.8 mL of pyrrole was injected into the ultra-sonicated colloid solution. Then, 6 g of $FeCl_3$ was added and the mixture was shaken manually for 5 min. For complete polymerization reaction to take place, the mixture was left to stand for three hours. The black powder obtained was filtered, washed with deionised water until the filtrate becomes colour less. To stop the reaction within the filtrate, acetone was injected. The magnetic nanocomposite was dried under vacuum at 60°C for 24 h to obtain a constant mass of the product.

2.3. Characterization of adsorbent

The synthesized PPy/Fe_3O_4 nanocomposite was characterised using the X-ray diffractometer to determine the XRD diffraction patterns using the SmartLab X-ray diffractometer operating at 45 kV/200 mA with Cu-Kα radiation (wavelength (λ) =1.540593). The FTIR spectra were obtained using a Perkin-Elmer Vertex 70 Spectrometer with a wavenumber range of 500–3000 cm^{-1}. A high-resolution transmission electron microscopy (JEOL JEM-2100) and scanning electron microscopy (Leo-Zeiss), which was coupled with energy dispersive X-ray (EDX) were used to determine the size morphology and elementary composition of the adsorbent. To determine the surface area and pore diameter of the adsorbent, the Brunauer Emmett-Teller (BET) was used at low-temperature nitrogen adsorption-desorption technique on a Micromeritics ASAP 2020 gas adsorption equipment (Micromeritics USA). The magnetic properties of the adsorbent were determined at room temperature using Bruker-Electron Spin Resonance (ESR) spectrometer and vibrating sample magnetometer (VSM) of the physical property measurement system (Quantum Design).

2.4. Experimental setup and method

The experimental setup is made up of a 1.1 kW three-phase induction motor having a stator winding of internal thickness and height of 14.39 × 160 mm, a rotor modified to hold an open-top toroidal cleaning chamber made from perspex plastic (internal, external and height diameters of 66 × 100 × 25 mm), a 10 A variable power source used as an AC power supply to the three-phase induction motor and a 220 V, 34 W fan mounted on a retort stand to maintain a uniform temperature within the system. Rotating magnetic field generated in the air-gap by the stator windings was measured using a digital gaussmeter (GM07/GM08 model), with a maximum magnetic field of 26.94 mT generated. The graphic representation of the magnetic field adsorption experimental setup is shown in Fig. 1.

To study the effect of pH on congo red adsorption onto magnetic nanocomposite influenced by a rotating magnetic field, 0.15 g adsorbent dosage was added to 50 mL congo red solutions (100 mg/L) with varying pH of 2–10 using 0.1 M NaOH/HCl solutions and spun in an anti-clockwise rotating magnetic field of 18.99 mT (The anti-clockwise magnetic field generated from the three-phase induction motor

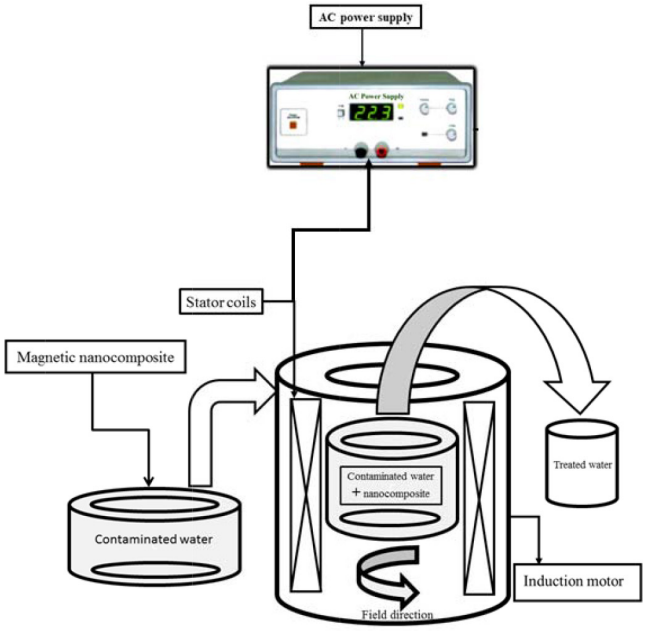

Fig. 1. Schematic diagram of magnetic adsorption device.

was used to physically stimulate the nanocomposite for CR adsorption, as it causes relative motion of the adsorption medium and the magnetic flux lines. It provides also more extensive use due to a possible variation of their frequency and exposure-time of the anti-clockwise rotating magnetic field). After the adsorption experiment, samples were centrifuged at 4000 rpm for 20 min using Lasec Hemle centrifuge to separate the dye solution from the adsorbent. The equilibrium congo red concentration was evaluated from a calibration curve using a UV/Vis spectrophotometer (PerkinElmer Lambda 1050) at an absorption wavelength of 497 nm. The removal efficiency was determined by computing the percentage sorption from Eq. (1). To determine the reproductivity of results reported, three independent sets of experiment were performed for each sample with their standard deviation reported. The standard deviation of the data is represented by errors bars incorporated in the figures.

$$\%\ Removal = \frac{C_o - C_e}{C_e} \times 100 \quad (1)$$

where the initial and equilibrium concentrations of congo red are represented by C_o and C_e (mg/L). The effect of adsorbent dosage on congo red adsorption influenced by a magnetic field was evaluated by contacting varying amounts of adsorbent dose (0.05–0.20 g) with 100 mg/L/50 mL of congo red solution adjusted to pH 4 and spun at a fixed magnetic field of 18.99 mT. The initial concentrations effect and adsorption isotherm on congo red adsorption were obtained by adding 0.15 g adsorbent dosage to 50 mL of initial congo red concentrations (100–400 mg/L) under the influence of a magnetic field of 18.99 mT for 24 h. The equilibrium adsorption capacity was evaluated using Eq. (2) below:

$$q_e = \frac{C_o - C_e}{m} \times V \quad (2)$$

where q_e (mg/g), V (L) and m (g) represent the amount of congo red absorbed per unit mass of the adsorbent, the volume of the sample and the adsorbent mass. Effect of the magnetic field applied on congo red adsorption was studied by contacting 0.15 g of adsorbent dosage with 50 mL of 100 mg/L congo red solution spun in varying magnetic field intensity of 11.84–26.94 mT. The magnetic exposure time effect on congo red adsorption was evaluated by contacting 0.15 g with 100 mg/L/50 mL of adsorbate which was exposed to a magnetic field at a fixed magnetic field of 18.99 mT for 10–120 min. For control purpose, magnetic exposure time experiments were also performed without magnetic field applied. The adsorption kinetics experiments were performed by contacting a fixed adsorbent dosage of 0.05 g with 50 mL congo red solution of initial concentrations (20–80 mg/L) at exposure time intervals of 10–120 min. The time-dependent amount of adsorbate adsorbed by a unit mass of adsorbent at the varying time was determined using Eq. (3):

$$q_t = \frac{C_o - C_t}{m} \times V \quad (3)$$

where q_t is the time-dependent amount of adsorbate adsorbed per unit mass of adsorbent (mg/g), C_t is the bulk phase concentration (mg/L) at any time t, V is the sample volume (L) and m is the adsorbent mass (g). To evaluate the adsorbent regeneration and recycling for congo red adsorption, adsorption-desorption experiments were performed. For the adsorption cycle study, 0.15 g adsorbent dosage was contacted with 100 mg/L of congo red solution at pH 4 and spun at a magnetic field of 18.99 mT. After the adsorption experiments, desorption experiments were performed to desorb the congo red from the adsorbent, by contacting 0.1 M of NaOH solution with the spent adsorbent, spun in the magnetic field of 18.99 mT for 60 min. To regenerate adsorption sites on the adsorbent after the desorption process, the adsorbent was treated with 2 M HCl spun in a magnetic field intensity of 18.99 mT for 60 min. Three successive adsorption-desorption experiments were performed to test the potential of re-using the adsorbent for congo red adsorption.

The pHpzc of the magnetic nanocomposite was determined by adjusting the pH value of 50 mL of 0.1 M NaCl solution in a series of Erlenmeyer flasks. The pH value was adjusted from 2–12 using either 0.1 M HCl or 0.1 M NaOH solution. Then 0.01 g of the magnetic nanocomposite was added to each flask and rotated at 18.99 mT for 120 min at room temperature. At the end of all experiments, the final pH was measured. The plot of final pH against initial pH was used in determining the pH_{pzc} of the adsorbent, where the values of the final pH and initial pH were constant. The effect of ionic strength on the adsorption of CR dye onto magnetic nanocomposite was evaluated by adding a varying concentration of NaCl salt (0.01–1 M) to 100 mg/L CR solution. 0.15 g of adsorbent was subsequently added and rotated in a magnetic field of 18.99 mT for 90 min. For co-existing anions effect on CR adsorption, 1 M of NaCl, Na_2So_4 and Na_2CO_3 were added to 100 mg/L CR solution. 0.15 g of adsorbent was then added and spun in a magnetic field of 18.99 mT for 90 mins. At the end of all experiments, the removal efficiency was determined by computing the percentage sorption using Eq. (1).

3. Results and discussion

The XRD patterns of the adsorbent (PPy/Fe_3O_4) before and after adsorption, magnetite (Fe_3O_4) and PPy which were normalised are shown in Figs. 2a–c. Diffraction peaks observed at 2θ value of 18.35(111), 30.14(220), 35.54(311), 43.18(400), 53.62(422), 57.06(511) and 62.68(440) corresponds to the cubic Fe_3O_4 phase (Fig. 2a), which was confirmed by the JCPDS file database (PDF No. 75-0449) [23,24]. A broad diffraction peak located at 2θ= 24.5 degree, which is a characteristic peak of amorphous PPy is observed in Fig. 2b [25]. It is also observed from the XRD result in Fig. 2c, that the Fe_3O_4 particles exist and was incorporated into the nanocomposite. The XRD pattern of the nanocomposite before and after adsorption of congo red dye was observed not to be affected by the induced magnetic field on the nanocomposite, as the nanocomposite crystalline structure did not change graphically after congo red adsorption.

FTIR spectra before and after adsorption of congo red by PPy/Fe_3O_4, Fe_3O_4, and PPy are shown in Fig. 3. The spectra of the magnetic adsorbent have characteristic peaks of the oxidised PPy and Fe_3O_4. Characteristic adsorption peak observed at 554 cm^{-1} was due to the vibration of the

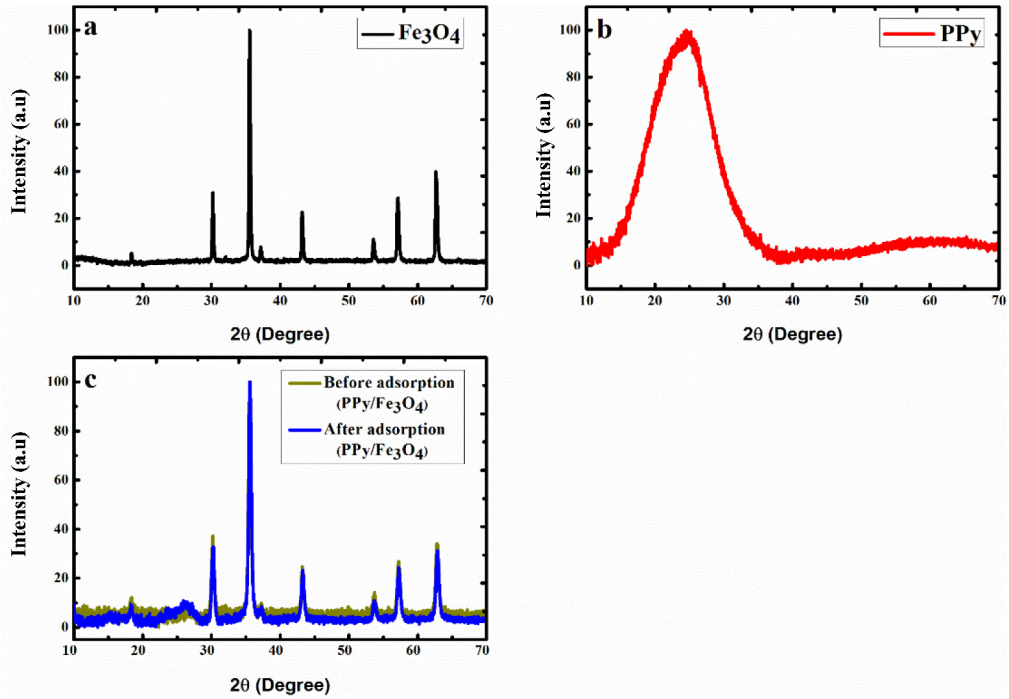

Fig. 2. XRD diffraction pattern of (a) Fe_3O_4, (b) PPy and (c) PPy/Fe_3O_4 nanocomposite before and after congo red adsorption.

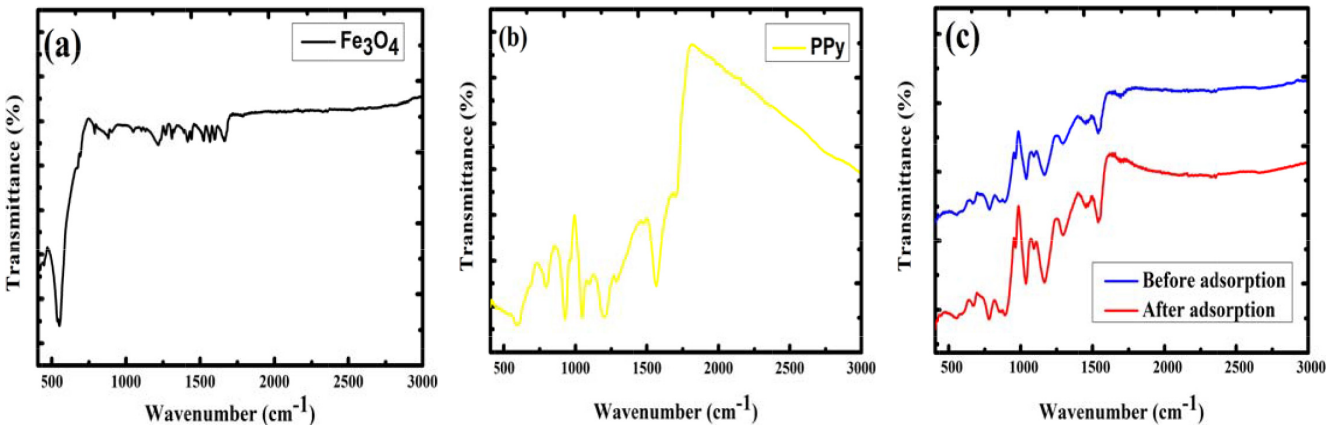

Fig. 3. FTIR spectra of (a) Fe_3O_4, (b) PPy and (c) PPy/Fe_3O_4 nanocomposite before and after adsorption.

Fe-O band, which is a characteristic peak of Fe_3O_4 (Fig. 3a) [26]. Adsorption peaks observed at 1543, 1458, 1290, 1173, 1034, 968 and 787 cm^{-1} were the characteristic peak of PPy in the nanocomposite before congo red adsorption (Fig. 3b). A shift to low adsorption values of the characteristic peak of PPy was observed after adsorption of congo red onto the PPy/Fe_3O_4 nanocomposite, with the PPy characteristic peaks shifting to 1537, 1454, 1286, 1159, 1030, 957 and 785 cm^{-1}. The adsorption peaks of PPy before and after adsorption of congo red corresponds to C=C stretch, C-N stretch, C-H or C-N in-plane deformation, C–C vibration, C-H in-plane deformation, C-C out of plane deformation vibration and out of plane C-H vibration of pyrrole. From the FTIR analysis, it is confirmed that PPy moiety is incorporated into the PPy/Fe_3O_4 nanocomposite. Reduction in the intensity of the adsorption peaks was observed after adsorption, which was due to CR adsorption onto the nanocomposite [25,27,28].

TEM and SEM images of the PPy/Fe_3O_4 nanocomposite are shown in Fig. 4. The SEM image shows spherical shape particles with a smooth uniform morphology caused by the deagglomerating effect of the polymer coating the nanoparticles. The diameter of particles ranges from 10–50 nm, with an average particle size distribution of 10.3 ± 8 and 10.4 ± 10 nm for TEM and SEM images analysis shown in Figs. 4a and b. The average particle size distribution obtained was fitted with the Gaussian function using the Image J software. From TEM image, Fe_3O_4 nanoparticles were observed to be encapsulated by the polymer matrix PPy, with the PPy/Fe_3O_4 nanocomposite being poly-dispersed. The morphology of the adsorbent also shows a core-shell structure with the Fe_3O_4 crystalline magnetic core being covered by

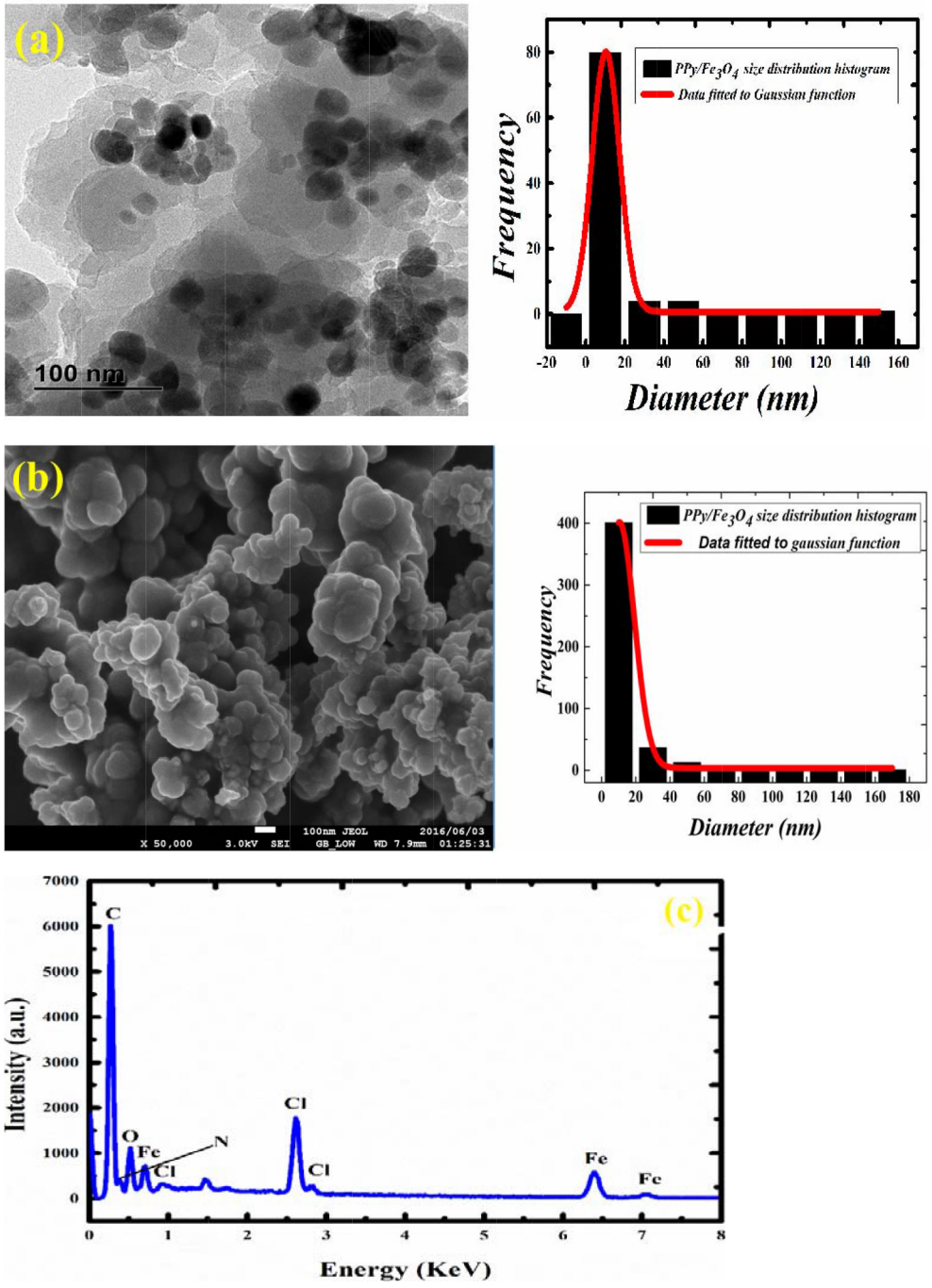

Fig. 4. (a) TEM of polypyrrole magnetic nanocomposite, with histogram obtained from the TEM showing the size distribution of the MNC fitted with a Gaussian fitting (b) SEM of polypyrrole magnetic nanocomposite, with histogram obtained from TEM showing the size distribution of the MNC fitted with Gaussian fitting (c) EDX spectra of PPy/Fe_3O_4 nanocomposite before adsorption.

the PPy shell (Fig. 4a). The EDX spectra (Fig. 4c) confirms the existence of C, O, N, Cl and Fe as the predominant elements in PPy/Fe_3O_4 nanocomposite with peaks observed at 0.27, 0.51, 0.36, 2.6, 0.69 and 6.39 keV. This confirms the incorporation of Fe_3O_4 into the polypyrrole polymer. The EDX analysis also shows that the PPy/Fe_3O_4 structure is composed of 58.54% carbon, 14.55% nitrogen, 5.71 chloride, 10.35% oxygen and 10.85% iron.

The nitrogen adsorption-desorption isotherm of PPy/Fe_3O_4 is shown in Fig. 5. The curve of the magnetic nanocomposite is a characteristic type-IV nitrogen adsorption-desorption isotherm, which describes a mesoporous material as categorized by IUPAC. The PPy/Fe_3O_4 nanocomposite has a hysteresis loop that closes at the relative pressure of 0.88 P/P_o. The BET surface area, BJH cumulative volume of pores and BJH average pore diameter of

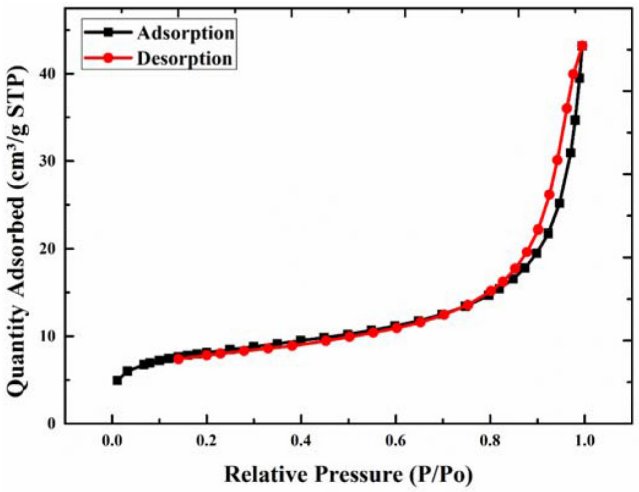

Fig. 5. N_2 adsorption–desorption isotherms of polypyrrole magnetic nanocomposite.

the magnetic nanocomposite were found to be 28.77 m²/g, 0.06 cm³/g and 15.82 nm. The tabulated values from the BET analysis is shown in Table 1 for polypyrrole magnetic nanocomposite [23,29,30].

The ESR spectra for magnetic nanocomposite before and after adsorption of congo red evaluated at room temperature are shown in Fig. 6. The line shapes are observed to be symmetrical, while the resonance signal is wide and broad with a line width value of approximately 1400 Gauss. The g-factor measurement of the unknown signal can be of valuable help in identifying a signal. For Fe^{3+} the g-factor is determined to be 1.4–3.1 for low spin and 2.0–9.7 for high spin complexes. The g-factor of the synthesized magnetic nanocomposite was found to be 2.25 Gauss, which was due to Fe^{3+} low spin interactions using Eq. (4);

$$g = \frac{hv}{\beta H_r} \tag{4}$$

where h is the Planck constant (6.626, × 10^{-27} *ere/s*) β is a universal constant (9.274 × 10^{-21} *Erg/G*), v is frequency (9.44 × 10^{9} *Hz*) and H_r is the resonance of magnetic field (3000 G). Such interactions show a super paramagnetic behaviour characterised by the presence of clusters. The shapes and the field location are identical to standard magnetic nanoparticle suspension and are consistent with ESR spectra of super paramagnetic iron oxide nanoparticles [31–34]. The line shape of the adsorbent before and after congo red adsorption was simulated using the Gaussian and Lorentzian functions. The line shape of the adsorbent was observed to fit well with Gaussian function (67%) than with Lorentzian function (31%) (Figs. 6b and c). This was a characteristic of ferromagnetic resonance (FMR) due to the dominant Gaussian function fitting (Fig. 6b) [35,36].

A plot of magnetisation (emu/g) vs magnetic field (Oe) measured at 300 K (Fig. 7) shows a magnetisation hysteresis loop with a zero-remanence magnetisation (H_r), coercivity field (H_c) and a saturation magnetisation (M_s) of 23 emu/g. The absence of hysteresis loops, remanence, and coercivity confirms that the polypyrrole magnetic nanocomposite is super paramagnetic. The saturation magnetisation of the

Table 1
Surface parameters of PPy/Fe_3O_4 nanocomposite

Sample	BET surface area ($m^2 \cdot g^{-1}$)	BJH cumulative Pore of volume ($cm^3 \cdot g^{-1}$)	BHJ average pore diameter (nm)
PPy/Fe_3O_4 nanocomposite	28.7688	0.063102	15.8235

nanocomposite is lower than those of magnetite, as the surface magnetic anisotropy is changed by the polypyrrole acting as a surfactant, which leads to an increase of the surface spins disorientation resulting in a decrease of the magnetic moment. This change is due to quantum size effects and increases in the surface area of the nanosized magnetite particles create super paramagnetic [37–39].

3.1. *Effect of pH on congo red adsorption influenced by magnetic field*

The key factor affecting the adsorption process is pH, as wastewater from textile industries has a range of pH values. The degree of ionisation of dye is also affected by pH. At pH 7, the colour of congo red in aqueous solution is solid red. This changes to blue-black and red at acidic and alkaline pH respectively [10–12]. This red colour is slightly different from the original red colour of congo red dye at neutral pH [40–42]. The point of zero charge (pH_{pzc}) of the polypyrrole magnetic nanocomposite was determined to be approximately 3.1 from Fig. S1. The surface charge of the adsorbent was positive at pH < pH_{pzc} and negative at pH > pH_{pzc} [43]. The point of acid constant (pKa) and the isoelectric point of CR were 4.1 and 3.0 at maximum adsorption wavelength (λmax) of 497 nm. At pKa of 4.1, CR molecules are negatively charged in the pH range of 5–10. CR is a dipolar molecule, which exist in cationic form at acidic pH, and anionic form at basic pH. The adsorption of cation is favourable at pH > $pH_{pzc,}$ while the adsorption of anions is improved at pH < pH_{pzc} [1,44–48]. The percentage of congo red dye removed was observed to increase as the pH value of congo red dye solution was increased from 2–4. A decrease in the amount of congo red dye removed was observed subsequently as the pH was increased from 6–10 (Fig. 8a). At pH 2, increase concentration of hydrogen ions in the solution promotes the build-up of ions on the nanocomposite adsorption sites (PPy/Fe_3O_4). This increase in protonation caused a strong repulsion between H^+ ions on the surface of PPy/Fe_3O_4 and the protonated congo red. Competition between protons (H^+) from the aqueous medium and congo red species for the adsorption site of PPy/Fe_3O_4 led to a suppressed removal of congo red at pH 2 [49,50]. The optimal pH for adsorption of congo red onto PPy/Fe_3O_4 nanocomposite from aqueous solution influenced by a magnetic field was determined to be pH 4. The adsorption of congo red dye onto the magnetic nanocomposite at pH attributed to the electrostatic attraction between the negatively charged adsorbent surface with the positively charged congo red dye (adsorbate), which exist in the cationic form in acidic medium. With increased pH (above pH 4),an increase OH^- ions on the adsorbent surface resulted in electrostatic

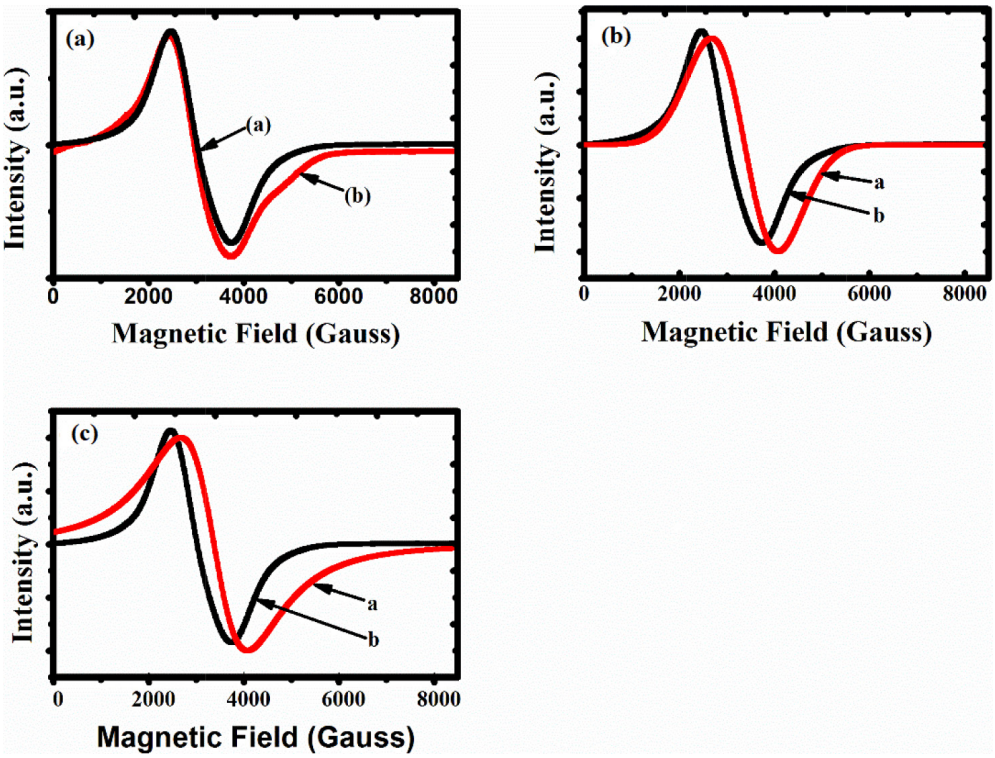

Fig. 6. (A)(1) ESR spectra of PPy/Fe_3O_4 nanocomposite after congo red adsorption and (2) before congo red adsorption, (B)(1) ESR spectra of PPy/ nanocomposite after congo red adsorption fitted to Gaussian fitting and (2) ESR spectra of PPy/Fe_3O_4 nanocomposite after congo red adsorption and (C)(1) ESR spectra PPy/Fe_3O_4 nanocomposite after congo red adsorption fitted to Lorentzian fitting and (2) ESR spectra PPy/Fe_3O_4 nanocomposite after congo red adsorption.

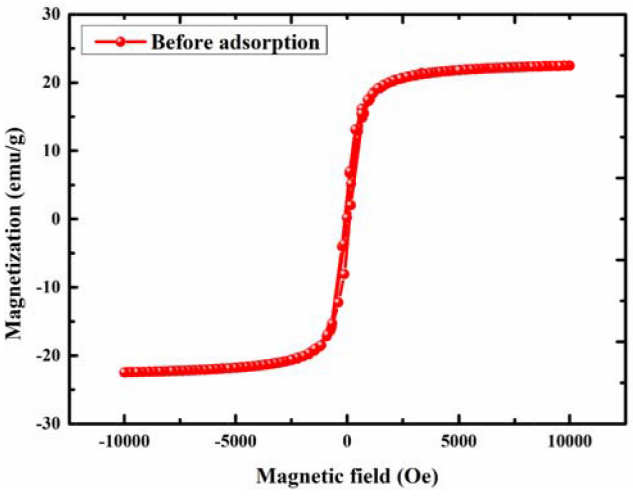

Fig. 7. M-H curve at room temperature for PPy/Fe_3O_4 nanocomposite.

repulsion between the negatively charged adsorbent with the negative congo red ions, as congo red has the property to aggregate in aqueous and organic solution. The aggregation phenomenon is important for high congo red concentrations at low pH. This is responsible for restriction of protonation of the functional groups from congo red at a low pH [51,52].

3.2. Effect of adsorbent dosage on congo red adsorption under magnetic field influence

A vital parameter that ascertains the capacity of an adsorbent for a given initial concentration of an adsorbate is adsorbent dosage. The adsorbent dosage is the most critical parameters for rapid and efficient dye removal [13,41]. It is observed from Fig. 8b, that the amount of congo red adsorbed by the adsorbent increased from 7–99% as the adsorbent dosage is increased from 0.05–0.20 g. Increased removal efficiency was related to the availability of extra active adsorption sites for congo red adsorption, which is directly related to the adsorbent mass. At low adsorbent dosage, the active adsorption sites are insufficient for the adsorbate to occupy. At high adsorbent dosage, the active adsorption sites are sufficient for the adsorbate to occupy, which leads to an increase in adsorption attributed to the increased adsorbent surface area and adsorption sites available.

3.3. Effect of initial concentration on congo red adsorption under magnetic field influence

The initial concentration effect on congo red adsorption under the influence of a magnetic field was examined at five different concentrations. As shown in Fig. 8c, increased in the initial congo red concentration (100–400 mg/L) leads to a decrease in the adsorption efficiency (100–88%). The ratio of available surface area to initial concentration of congo

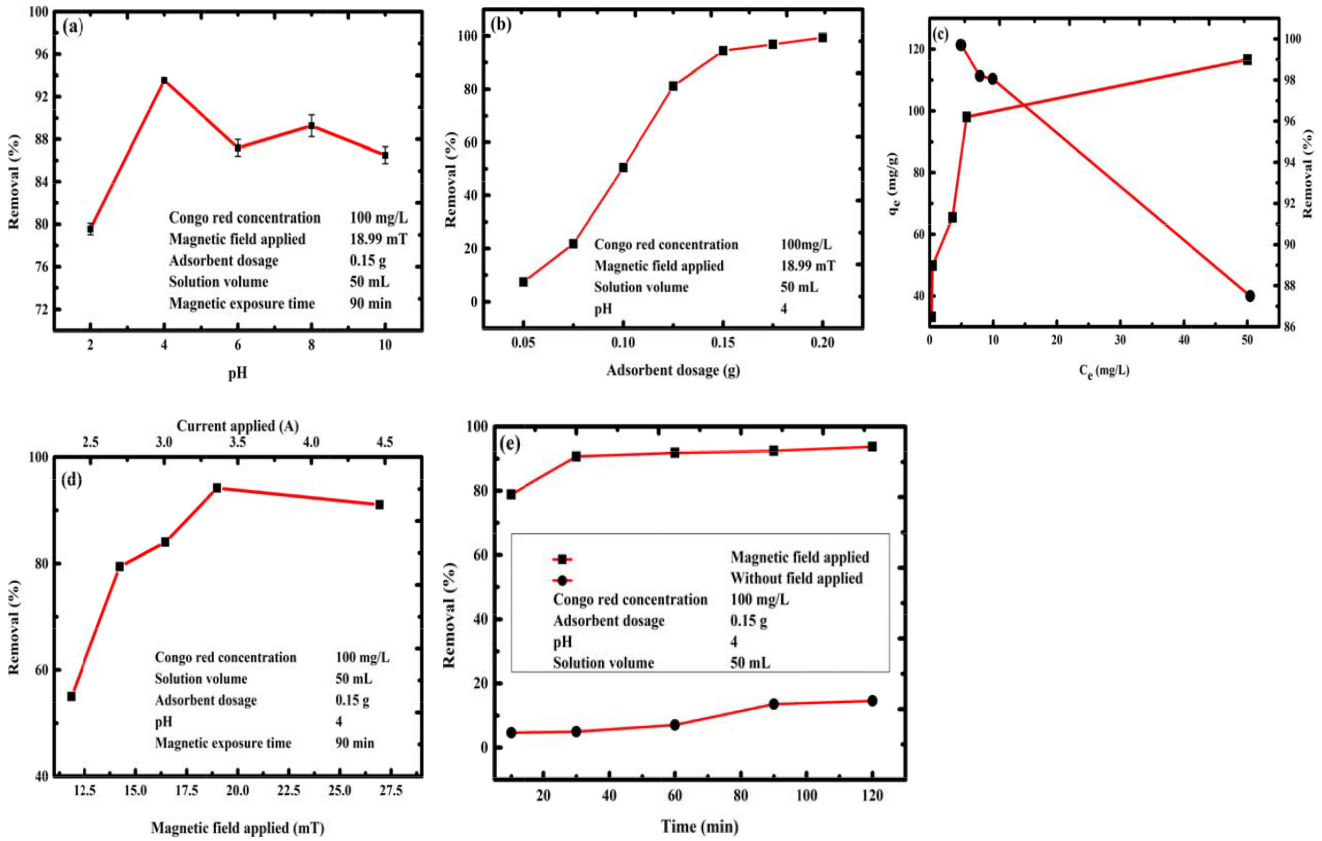

Fig. 8. (a) pH effect on congo red adsorption under the influence of MF (experimental parameters: adsorbent dosage 0.15 g, solution volume 50 mL, initial concentration of congo red solution 100 mg/L, pH 2–10, magnetic field 18.99 mT and magnetic exposure time 90 min), (b) Adsorbent dosage effect on CR adsorption under MF influence (experimental parameters: adsorbent dosage 0.05–0.20 g, solution volume 50 mL, initial concentration of congo red solution 100 mg/L, pH 4, magnetic field 18.99 mT and magnetic exposure time 90 min), (c) Initial concentration effect on CR adsorption under MF influence (experimental parameters: adsorbent dosage 0.15 g, solution volume 50 mL, initial concentration of congo red solution 100–400 mg/L, pH 4, magnetic field 18.99 mT and magnetic exposure time 1440 min), (d) Effect of magnetic field intensity on the adsorption of CR (experimental parameters: adsorbent dosage 0.15 g, solution volume 50 mL, initial concentration of congo red solution 100 mg/L, pH 4, magnetic field 11.84–26.94 mT, and magnetic exposure time 90 min) and (e)(a) Effect of magnetic exposure time on adsorption of CR and (b) without field applied on adsorption of CR (experimental parameters: adsorbent dosage 0.15 g, solution volume 50 mL, initial concentration of congo red solution 100 mg/L, pH 4, magnetic field 11.84 mT, and magnetic exposure time 20–120 min).

red is high at low concentrations; thereby adsorption efficiency tends to increase as the initial concentration of the adsorbate is inversely related to the adsorption efficiency. As the initial concentration increases, efficiency decreases. The quantity of congo red absorbed per unit mass of the adsorbent increased from 33–117 mg/g as the equilibrium concentration of the adsorbate increased from 0.3–50 mg/L for initial concentrations of 100–400 mg/L. The high driving force for mass transfer in high dye concentrations causes an increase in the adsorption capacity as the initial concentration is increased [52].

3.4. Effect of magnetic field and exposure time on congo red adsorption

Results from the adsorption of congo red dye onto polypyrrole magnetic nanocomposite influenced by the magnetic field of different intensity and magnetic exposure time are shown in Figs. 8d, e. Increased percentage of congo red ions adsorbed onto polypyrrole magnetic nanocomposite under the influence of increasing magnetic field was observed, with 55–94% removal attained with an increase in magnetic field intensity of 11.84–26.94 mT, the maximum removal of congo red observed at 18.99 mT. From the magnetic exposure time result, 79–94% of congo red dye was observed to be removed with an increased magnetic exposure time of 10–120 min at a constant magnetic field of 18.99 mT. When no field was applied (control), the amount of congo red dye adsorbed onto the adsorbent was observed to be 5–15%. Increase in the percentage removal under the influence of magnetic field was ascribed to the improved size of particles aggregates as the magnetic field influence on the magnetic nanocomposite was increased from low magnetic field to high magnetic field intensity. The aggregates size was observed to depend on the magnetic velocity, with fast moving even particles aggregates with a large surface area observed at high magnetic field. Small non-uniform particles aggregates travelling with slow point velocities was observed at low magnetic field, with a reduced surface area. Chain breakage in the aggregates was noticed to meaningfully reduces the swimming efficiency of

the particles at low magnetic field, leading to the reduced surface area for the adsorption. The lateral binding of chains driven into contact by magnetic manipulations substantially increases the chain polydispersity, hence increased chain collision and area of particle interaction [22,53].

3.4.1. Adsorption isotherms

The interaction between the adsorbate molecules and the adsorbent surface is best described by adsorption isotherm models. To optimise the design of adsorption systems, a suitable correlation for equilibrium curves is essential [52,54]. Thus, congo red adsorption onto polypyrrole magnetic nanocomposite was ascertained as a function of congo red equilibrium concentration (C_e) and the related adsorption isotherm plotted in Fig. 9. To study the adsorption of the adsorbate, Langmuir and Freundlich isotherm models were adjusted with the isotherm data. The Langmuir adsorption isotherm model assumes that the adsorptions occur at specific homogeneous sites on the adsorbent. It is successfully used in many monolayer adsorption processes. The non-linear and linearize forms of the Langmuir equation are represented by the following equations:

$$q_e = \frac{q_m b C_e}{1 + bC_e} \tag{5}$$

$$\frac{C_e}{q_e} = \frac{1}{qm^b} + \frac{C_e}{q_m} \tag{6}$$

The maximum mono layer adsorption capacity, the equilibrium dye concentration and the Langmuir isotherm constant related to the affinity of the binding sites are represented by q_m (mg/g), C_e (mg/L) and b (L/mg). An additional analysis of the Langmuir equation is made on the fundamentals of a dimensionless equilibrium parameter (R_L), also known as separation factor, which is defined as:

$$R_L = \frac{1}{1 + bC_0} \tag{7}$$

where C_o is initial adsorbate concentration (mg/L), R_L values indicate whether the adsorption process is irreversible ($R_L = 0$), favourable ($0 < R_L < 1$), linear ($R_L = 1$), or unfavourable ($R_L > 1$) [55]. Freundlich isotherm is an empirical model based on the assumption of the heterogeneous surface with a non-uniform adsorption heat distribution over the surface of the adsorbent. The non-linearize and linearize form of Freundlich isotherm is given by the following equations:

$$q_e = k_f C_e^{\frac{1}{n}} \tag{8}$$

$$Inq_e = Ink_F + \frac{1}{n} InC_e \tag{9}$$

The adsorption capacity and intensity of adsorption constants are associated with k_F and $1/n$ [20,56]. Fig. 9a, b shows the linearized forms of Langmuir and Freundlich isotherms models. Parameters for Langmuir and Freundlich isotherms models were estimated from plots for C_e/q_e vs C_e. and $In\ q_e$ vs $In\ C_e$. respectively at a solution temperature of 31 ± 1°C. Based on the correlation coefficient values for the two models, the higher correlation coefficient value for the Langmuir isotherm model (R^2=0.99977) fitted well to the experimental data very well when compared to Freundlich isotherm model (R^2=0.85488). This indicates a homogeneous distribution of the active sites on the surface of the polypyr role magnetic nanocomposite and the chemical adsorption between congo red and the nanocomposite. The values of the Langmuir equilibrium coefficient, 'b', Langmuir maximum mono layer adsorption capacity and the dimensionless separation factor 'R_L' were estimated to be 0.72 L/g, 119.76 mg/g and 0.014 respectively, with the dimensionless separation factor 'R_L' signifying that the adsorption process is favourable. The Freundlich parameters k_F and n values are 52.52 and 4.34. The intensity of adsorption constant (n) from the Freundlich isotherm is greater than 1, which shows a favourable adsorption. The Langmuir and Freundlich isotherm parameters calculated from the slope and intercept of the linear equations are shown in Table 2. The maximum adsorption capacity (q_m) of congo red onto PPy/Fe_3O_4 nanocomposite was calculated from the Langmuir isotherm to be 119.76 mg/g. This was

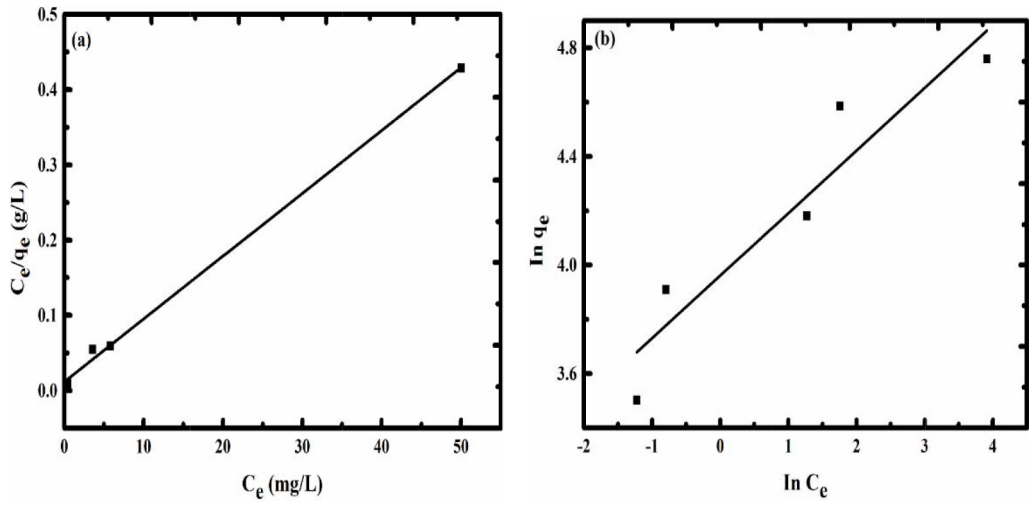

Fig. 9. (a) Fit of equilibrium data to the Langmuir isotherm model (b) Fit of equilibrium data to Freundlich isotherm model.

Table 2
Langmuir and Freundlich isotherm constants for adsorption of congo red dye on 0.15 g PPy/Fe_3O_4 nanocomposite

Temperature	Langmuir constant				Freundlich constant		
31± 1°C	q_m	b	R_L	R_2	k_f	n	R^2
	119.76	0.72	0.014	0.99977	52.52	4.34	0.85488

Table 3
Comparison of congo red adsorption capacity of PPy/Fe_3O_4 nanocomposite with other reported adsorbents

Adsorbent	q_m (mg/g)	Optimum pH	Reference
SPS/MNPs	71.4	7	57
PAn/TiO_2 nanocomposite	80.7	6	58
Iron oxide/carbon nanocomposites	105.3	-	59
Leucaena leucocephala (Subabul) seed pods	4.4	5	13
$Al_2O_3/Ni_{0.5}Zn_{0.5}Fe_2O_4$ Microfibers	75.5	6.5	60
Magnetic iron oxide nano powder	54.5	6	61
Chitosan/ montmorillonite nanocomposite	54.5	4	62
PPy/Fe_3O_4 nanocomposite	119.8	4	Present study

compared with other reported magnetic adsorbents shown in Table 3. The maximum adsorption capacity of the PPy/Fe_3O_4 nanocomposite was observed to be significantly higher than the capacity of other adsorbents. Hence, owing to PPy/Fe_3O_4 nanocomposite high adsorption capacity, simple synthesis process and magnetic properties makes PPy/Fe_3O_4NC a promising adsorbent for CR adsorption.

3.4.2. Adsorption kinetics

The rate of solute uptake governs the adsorption reaction residence time, best described by the adsorption kinetics [63]. The exposure time was varied from 10–120 min with initial congo red concentrations of 20–80 mg/L. The congo red dye uptake was analysed at different magnetic exposure time intervals as shown in Fig. 10a. Congo red adsorption was fast and improved with an increase in magnetic exposure time and initial concentration, with equilibrium attained at 40–120 min under the influence of a magnetic field. To understand the mechanism of congo red adsorption onto the adsorbent, the pseudo-first-order and pseudo-second-order model were used to fit the kinetics data. The linearize forms of the pseudo-first-order and pseudo-second-order kinetics equations are:

$$\log(q_e - q_t) = \log q_e - \frac{k_1}{2.303}t \quad (10)$$

$$\frac{t}{q_t} = \frac{1}{k_2 q_e^2} + \frac{1}{q_e}t \quad (11)$$

The congo red uptake at time t, the pseudo-first and second order rate constants are represented by q_t (mg/g), k_1 and k_2 (1/min). The linear plot of Eqs. (10) and (11) are shown in Figs. 10b, c. From the plot, the rate constants and the correlation coefficients were determined given in Table 4. The correlation coefficients of the pseudo-second-order model gave a better explanation of the congo red dye adsorption onto PPy/Fe_3O_4 (R^2 = 0.99959, 0.99936 and 0.99347) when equated to the pseudo-first-order model (R_2 = 0.96798, 0.95031 and 0.95280), which indicates that the kinetics of congo red dye adsorption onto PPy/Fe_3O_4 was governed by this model (pseudo-second order), with the rate constants (K^2) decreasing from 0.024–0.003 g·min/mg with an increase in congo red dye initial concentration. The equilibrium sorption uptake were 18.66, 29.79 and 39.05 mg/g for the linear pseudo-second-order model under a magnetic field applied influence. Thus, the adsorption capacity (q_e) from the experimental values fits very well with the theoretical adsorption capacity ($q_{e'}$ *cal*) values calculated from the pseudo-second-order model. The trend of equilibrium sorption uptake ($q_{e'}$) values obtained from the linear fit of the pseudo-second-order model showed an increase with an increase in initial concentration, which is attributed to adsorption being a passive process, driven specifically by concentration gradient as a driving force [64]. These results confirm that congo red adsorption kinetics can be better be defined by the pseudo-second-order model.

3.5. Effect of ionic strength

An important parameter that controls the electrostatic and non-electrostatic interactions between the adsorbate (CR dye) and the adsorbent surface is the ionic strength of the solution [65]. The effect of ionic strength on the adsorption of CR dye onto PPy/Fe_3O_4 was investigated by adding a varying concentration of NaCl to 100 mg/L of CR solution at pH 4. The result shown in Fig. S2 shows an increase in the removal of CR dye with increased concentration of NaCl from 0.01–1 M. Usually, increase in the ionic strength decreases the percentage removal due to the presence of electrostatic screening. But the experimental data did not follow this tendency, as this was ascribed to induced aggregation of the molecules of CR induced by NaCI ions enhancing the extent of adsorption by the adsorbent [66].

3.6. Effect of co-existing anions

Considering natural water sources intricacy, several anions exist with CR in wastewater and might affect the removal efficiency of an adsorbent to remove CR [67]. Selected anions CI^-, SO_4^{2-}, and CO_3^{2-} were analyzed to evaluate their effect on the removal of CR onto polypyrrole magnetic nanocomposite (Fig. S3). The result shows that co-existing mono or divalent anions did not have any significant effect on the adsorption of CR dye onto polypyrrole magnetic nanocomposite. It was observed that the presence of CI^-, SO_4^{2-}, and CO_3^{2-} increased the percentage

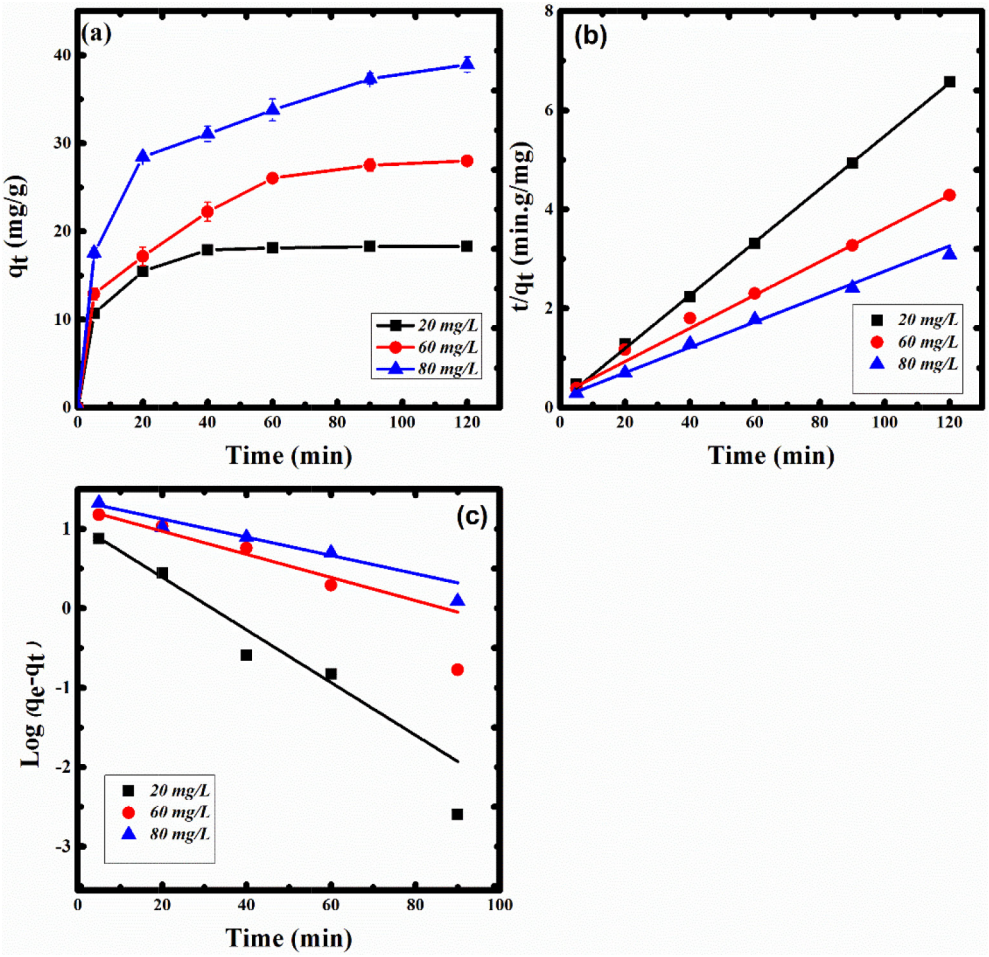

Fig. 10. (a) Kinetics data for CR adsorption onto PPy/Fe_3O_4 (b) Pseudo first order model for adsorption of CR onto PPy/Fe_3O_4 (c) Pseudo-second order model for adsorption of CR onto PPy/Fe_3O_4 .

Table 4
Kinetics parameters for adsorption of congo red ions from aqueous medium

C_e mg/L	Pseudo-first order model			Pseudo-second order model		
	K_1 (1/min)	q_e (mg/g)	R^2	k_2 (g/mg/min)	q_e (mg/g)	R^2
20	0.076	11.34	0.96798	0.024	18.66	0.99959
60	0.034	18.31	0.95031	0.004	29.79	0.99936
80	0.027	22.67	0.95200	0.003	39.05	0.99347

of CR dye removal to 97.7%, 96.4% and 95.9%. This may be attributed to an increase in the ionic strength of the solution. CR removal in the presence of anions increased in the order of $Cl^- > SO_4^{2-} > CO_3^{2-}$.

3.7. Reuse of pre-treated PPy/Fe_3O_4

The potential for recycling of adsorbent is a very important parameter to assess their practicability. If a strong base such as NaOH can desorb the dye, it can be said that the attachment of the dye to the adsorbent is ion exchange [68]. NaOH was used for the elution of congo red dyes from PPy/Fe_3O_4 for three cycles to desorb congo red adsorbed on the surface of PPy/Fe_3O_4 after adsorption. To regenerated adsorption sites after desorption of congo red dye with NaOH, the adsorbent is subsequently treated with 2 M HCl. The results of the adsorption-desorption process using NaOH is shown in Fig. 11. It is observed that congo red removal remains constants (96%) up to the second cycle and that there is a slight drop in the congo red removal at the third cycle (94%). The slight decrease in removal may be due to breakage of the polymer chain by repeated acid/base treatment of the nanocomposite during the regeneration process [69].

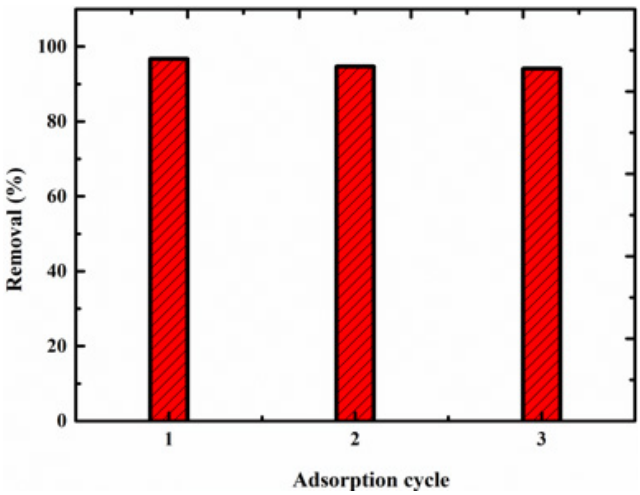

Fig. 11. Adsorption-desorption cycles (experimental parameters: adsorbent dosage 0.15 g, initial concentration of congo red solution 100 mg/L, pH 4, magnetic field 18.99 mT and magnetic exposure time 60 min).

4. Conclusions

We used the newly developed purification technique based on the motion of functionalized magnetic nanoparticles in the congo red contaminated water by the time alternating magnetic poles in a modified electric motor. Enhanced removal of congo red from aqueous solutions onto polypyrrole magnetic nanocomposite under the influence of magnetic field and magnetic exposure time was observed, with percentage removal of 94% under the influence of magnetic field. The increase in removal efficiency was due to the magnetic force applied when a charged particle passed through a magnetic field, thereby realigning the magnetic moment of either the adsorbent or adsorbent for quick adsorption. From kinetics and adsorption isotherm models, it is observed that there was significantly enhanced adsorption of congo red, as the initial concentration is increased. The pseudo-second model best describes the adsorption of congo red onto the adsorbent. The equilibrium adsorption capacity obeys the Langmuir isotherm with a maximum adsorption capacity of 119.76 mg/g. The maximum adsorption capacity of PPy/Fe_3O_4 was observed to be significantly higher than the adsorption capacity of other magnetic adsorbents reported by other researchers due to its low cost, simple synthesis process, high uptake capacity, and unique magnetic property that allows for the adsorbent to be simulated physically by the rotating magnetic field for CR dye adsorption, making it a unique adsorbent for CR adsorption.

Acknowledgements

The authors are thankful for the financial support from the Research and Innovation Directorate of UNISA through the Innovation Support Programme, National Centre for Nanostructured Materials, South Africa Council for Scientific and Industrial Research, Pretoria, Dr M. Bhaumik and Dr Raghunath Das for their support and advice.

References

[1] F. Ferrarini, I.R. Bonetto, J.S. Crespo, M. Giovanela, Removal of congo red dye from aqueous solutions using a halloysite-magnetite-based composite, Water Sci. Technol., 73 (2016) 2132–2142.
[2] A.A. Tireli, F.C.F. Marcos, L.F. Oliveira, L. Do, R. Guimaraes, M.C. Guerreiro, J.P. Silva, Influence of magnetic field on the adsorption of organic compound by clays modified with iron, Appl. Clay Sci., 97 (2014) 1–7.
[3] O.F.G. Vazquez, M.M. Virgen, V.H. Montoya, R.T. Gomez, J.L.A. Flores, M.P. Cruz, M.A.M. Moran, Adsorption of heavy metals in the presence of a magnetic field on adsorbents with different magnetic properties. Ind. Eng. Chem. Res., 55 (2016) 9323–9331.
[4] A. Afkhami, R. Moosavi, Adsorptive removal of congo red, a carcinogenic textile dye, from aqueous solutions by maghemite nanoparticles. J. Hazard Mater., 174 (2010) 398–403.
[5] H. Kaur, S. Kaur, R. Kaur, Kinetic and isotherm studies of congo red adsorption from aqueous solution by biowaste material. Chem. Sci. Trans., 3 (2014) 1300–1309.
[6] W.B. Mbarek, M. Azabou, E. Pineda, N. Fiol, L. Escoda, J.J. Sunol, M. Khitouni, Rapid degradation of azo-dye using Mn–Al powders produced by ball-milling. RSC Adv., 7 (2017) 12620–12628.
[7] A. Mittal, L. Kurup, J. Mittal, Freundlich and Langmuir adsorption isotherms and kinetics for the removal of tartrazine from aqueous solutions using hen feathers. J. Hazard Mater., 146 (2007) 243–248.
[8] Y. Wu, H. Luo, H. Wang, Efficient removal of congo red from aqueous solutions by surfactant-modified hydroxo aluminum/graphene composites, Sep. Sci. Technol., 49 (2014) 2700–2710.
[9] C. Jiang, B. Fu, H. Cai, T. Cai, Efficient adsorptive removal of congo red from aqueous solution by synthesized zeolitic imidazolate Framework-8, Chem. Spec. Bioavailab., 28 (2016) 199–208.
[10] D. Hu, P. Weng, J. Li, L. Wang, Functionalization of micro crystalline cellulose with N, N-dimethyldodecylamine for the removal of congo red dye from an aqueous solution, Bioresour., 9 (2014) 5951–5962.
[11] A. Karamipour, N. Rasouli, M. Movahedi, H. Salavati, A kinetic study on adsorption of congo red from aqueous solution by ZnO-$ZnFe_2O_4$-polypyrrole magnetic nanocomposite, Phys. Chem. Res., 4 (2016) 291–301.
[12] Z. Chen, H. Deng, C. Chen, Y. Yang, H. Xu, Biosorption of malachite green from aqueous solutions by Pleurotus Ostreatus using Taguchi method, J Environ. Health Sci. Eng., 12 (2014) 63.
[13] V.S. Shrivastava, Removal of congo red dye from aqueous solution by Leucaena Leucocephala (Subabul) seed pods. Int. J. Chem. Tech. Res., 4 (2012) 1038–1043.
[14] J. Si, T. Yuan, B. Cui, Exploring strategies for adsorption of azo dye congo red using free and immobilized biomasses of Trametes Pubescens, Ann Microbiol., 65 (2015) 411–421
[15] O.V. Makarchuk, T.A. Dontsova, I.M. Astrelin, Magnetic nanocomposites as efficient sorption materials for removing dyes from aqueous solutions, Nano. Res. Lett., 11 (2016) 161–168.
[16] Y. Ali, R. Samaneh, R. Zohre, J. Mostafa, Magnetic water treatment in environmental management: a review of the recent advances and future perspectives. Curr. World Environ., 9 (2014) 1008–1016.
[17] R.A. Barrett, S.A. Parsons, The influence of magnetic fields on calcium carbonate precipitation. Water Resour., 32 (1998) 609–612.
[18] P.L. Hariani, M. Faizal, R. Seliabudidaya, M. Seliabudidaya, D. Setiabudidaya, Synthesis and properties of Fe_3O_4 nanoparticles by co-precipitation method to removal Procion dye. Int. J.Environ. Sci. Develop., 4 (2013) 336–340.
[19] M.M.K. Alkhazan, A.A.N. Saddiq, The effect of magnetic field on the physical, chemical and microbiological properties of the lake water in Saudi Arabia, J. Evol. Biol. Res., 2 (2010) 7–14.
[20] G. Li, W. Zhu, C. Zhang, S. Zhang, L. Liu, L. Zhu, W. Zhao, Effect of a magnetic field on the adsorptive removal of Methylene Blue onto wheat straw biochar, Bioresour. Technol., 206 (2016) 16–22.

[21] J. Bogatin, N.P. Bondarenko, E.Z. Gak, E.E. Rokhinson, I.P. Ananyev, Magnetic treatment of irrigation water: experimental results and application conditions. Environ. Sci. Technol., 33 (1999) 1280–1285.
[22] U.O. Aigbe, R. Das, W.H. Ho, V. Srinivasu, A. Maity, A novel method for removal of Cr(VI) using polypyrrole magnetic nanocomposite in the presence of unsteady magnetic fields, Sep. Purif. Technol., 194 (2018) 377–387.
[23] B. Kakavandi, B.R. Kalantary, A.J. Jafari, S. Nasseri, A. Ameri, A. Esrafili, A. Azari, Pb(II) Adsorption onto a magnetic composite of activated carbon and super paramagnetic Fe_3O_4 nanoparticles: experimental and modelling study. Clean Soil Air Water, 43 (2015) 1157–1166.
[24] K. Suri, S. Annapoorni, R.P. Tandon, Phase change induced by polypyrrole in iron-oxide polypyrrole Nanocomposite. B. Mater. Sci., 24 (2001) 563–567.
[25] J. Guo, H. Gu, H. Wei, Q. Zhang, N. Haldolaarachchige, Y. Li, D.P. Young, S. Wei, Z. Guo, Magnetite–polypyrrole meta composites: dielectric properties and magneto resistance behaviour. J. Phys. Chem., 117 (2013) 10191–10202.
[26] R. Turcu, O. Pana, A. Nan, I. Craciunescu, O. Chauvet, C. Payen, Polypyrrole coated magnetite nanoparticles from water based nanofluids. J. Phys. D., 41 (2008) 2450–2452.
[27] S. Kasisomayajula, N. Jadhav, V.J. Gelling, In situ preparation and characterization of a conductive and magnetic nanocomposite of polypyrrole and copper hydroxy chloride. RSC. Adv., 6 (2016) 967–977.
[28] F. Khalilian, M. Rezaee, M.K. Gorgabi, Magnetic polypyrrole/Fe_3O_4 particles as an effective sorbent for the extraction of abamectin from fruit juices using magnetic solid-phase extraction combined with dispersive liquid-liquid micro extraction. Anal. Methods., 7 (2015) 2182–2189.
[29] K. Zhu, C. Chen, H. Xu, Y. Gao, X. Tan, A. Alsaedi, T. Hayat, Cr(VI) Reduction and immobilization by core-double-shell structured magnetic polydopamine/zeolite idazolate Frameworks-8 Micro sphere. ACS Sustain Chem. Eng., 5 (2017) 6795–6802.
[30] M.H. Mohamed, M. Pirlot, M.K. Danquah, L.D. Wilson, Use of industrial coal waste materials as adsorbents for textile effluent remediation. J. Mater. Sci. Chem. Eng., 5 (2007) 12–24.
[31] R. Sivashankar, A.B. Sathya, V. Vasatharaj, V. Sivasubramanian, Magnetic composite an environmental super adsorbent for dye sequestration–a review. ENMM, 1 (2014) 36–49.
[32] B. Chertok, A.J. Cole, A.E. David, V.C. Yang, Comparison of electron spin resonance spectroscopy and inductively-coupled plasma optical emission spectroscopy for bio distribution analysis of iron-oxide nanoparticles, Mol. Pharm., 7 (2010) 375–385.
[33] Y. Koseoglu, F. Yildiz, D.K. Kim, M. Muhammed, B. Aktas, EPR studies on Na-oleate coated Fe_3O_4 nanoparticles, Physica Status Solidi, 12 (2004) 3511–3515.
[34] J.B. Mamani, I.F. Gamarra, G.E. De Souza Brito, Synthesis and characterization of Fe_3O_4 nanoparticles with perspectives in biomedical applications, Mat. Res., 17 (2014) 542–549.
[35] M. Bhaumik, T.Y. Leswifi, A. Maity, V.V. Srinivasu, M.A. Onyango, Removal of fluoride from aqueous solution by polypyrrole/Fe_3O_4 magnetic nanocomposite. J. Hazard Mater., 186 (2011) 150–159.
[36] O.A. Kuznetsov, O.N. Sorokina, V.G. Leontiev, O.A. Shlyakhtin, A.L. Kovarski, A.A. Kuznetsov, ESR study of thermal demagnetization processes in ferromagnetic nanoparticles with Curie temperatures between 40 and 60, J. Magn. Magn. Mater., 311 (2007) 204–207.
[37] T. Theivasanthi, M. Alagar, Innovation of super paramagnetism in lead nanoparticles, cond-mat.mtrl-sci. arXiv:1402–1431.
[38] A.M. Muliwa, M.S. Onyango, Efficient removal of Cr (VI) from aqueous solution with PPy-Fe_3O_4 nanocomposite, Proc. Sustain. Res. Innov., 5 (2014) 83–90.
[39] N. Shamim, L. Hong, K. Hidajat, M.S. Uddin, Thermosensitive-polymer-coated magnetic nanoparticles: adsorption and desorption of bovine serum albumin, J. Colloid Interface Sci., 304 (2006) 1–8.
[40] Z. Hu, H. Chen, F. Ji, S. Yuan, Removal of congo red from aqueous solution by cattail root. J. Hazard Mater., 173 (2010) 292–297.
[41] M. Ghaedi, S. Ramazani, M. Roosta, Gold nanoparticle-loaded activated carbon as novel adsorbent for the removal of Congo Red. Indian J. Sci. Technol., 4 (2011) 1208–1217.
[42] L. Dong, Z. Zhipeng, D. Yigang, A simple method to prepare magnetic modified corncobs and its application for congo red adsorption. J. Disp. Sci. Technol., 37 (2016) 73–79.
[43] S. Wei, X. Hu, H. Liu, Q. Wang, C. He, Rapid degradation of congo red by molecularly imprinted polypyrrole-coated magnetic TiO_2 nanoparticles in dark at ambient conditions, J. Hazard Mater., 294 (2015) 168–176.
[44] A.T. Ojedokun, O.S. Bello, Kinetic modelling of liquid-phase adsorption of Congo Red dye using guava leaf-based activated carbon, Appl. Water Sci., 7 (2017) 1965–1977.
[45] Z.L. Yaneva, N.V. Georgieva, Insights into congo red adsorption on agro-industrial materials-spectral, equilibrium, kinetic, thermodynamic, dynamic and desorption studies. A Review, Inter. Review of Chem. Eng., 4 (2012) 127–146.
[46] N. Rasouli, A. Khalili, Enhanced adsorption capability of Congo Red dye onto novel polypyrrole/ZnO/$ZnCr_2O_4$ composite, Chem. Res. J., 2 (2017) 1–10.
[47] Y. Wu, H. Luo, H. Wang, Efficient removal of congo red from aqueous solutions by surfactant-modified hydroxo aluminum/graphene composites, Sep. Sci. Technol., 49 (2014) 2700–2710.
[48] T.A. Ojo, A.T. Ojedokun, O.S. Bello, Functionalization of powdered walnut shell with orthophosphoric acid for congo red dye removal, Partic. Sci. Technol., (2017) 1–12.
[49] R. Satheesh, K. Vignesh, M. Rajarajan, A. Suganthi, S. Sreekantan, M. Kang, B.S. Kwak, Removal of Congo Red from water using quercetin modified α-Fe_2O_3 nanoparticles as effective nano adsorbent. Mater. Chem. Phys., 180 (2016) 53–65.
[50] T.V. Toledo, C.R. Bellato, C.H. Ferreira de Souza, J.T. Domingues, D.D.C. Silva, C. Reis, P.F. Fontes, Preparation and evaluation of magnetic chitosan particles modified with ethylenediamine and Fe (III) for the removal of Cr (VI) from aqueous solutions, Quimica Nova, 37 (2014) 1610–1617.
[51] B. Gurunanthan, D. Viswanathan, S. Rajasekar, G.B. George, Magnetic nanocomposite of activated charcoal for removal of Congo Red dye. Manage. Environ. Qual., 27 (2016) 45–58.
[52] H. Chen, J. Zhao, Adsorption study for removal of congo red anionic dye using organo-attapulgite. Adsorption., 15 (2009) 381–389.
[53] U.O. Aigbe, W.H. Ho, A. Maity, M. Khenfouch, V. Srinivasu, Removal of hexavalent chromium from wastewater using PPy/Fe_3O_4 magnetic nanocomposite influenced by rotating magnetic field from two pole three-phase induction motor. J. Physics: Conf. Series, 984 (2018) 012008.
[54] B. Saha, S. Das, J. Saiki, G. Das, Preferential and enhanced adsorption of different dyes on iron oxide nanoparticles: a comparative study, J. Phys. Chem., 115 (2011) 8024–8033.
[55] W.C. Wanyonyi, J.M. Onyari, P.M. Shiundu, Adsorption of Congo Red dye from aqueous solutions using roots of Eichhornia Crassipes: Kinetic and equilibrium studies, Energy. Procedia., 50 (2014) 862–869.
[56] A. Shojamoradi, H. Abolghasemi, M. Esmaili, Foroughi-Dahr H. Fatoorechi, Experimental studies on congo red adsorption by tea waste in the presence of silica and Fe_2O_3 nanoparticles, J. Pet. Sci. Technol., 3 (2013) 25–34.
[57] A.M. Al-Sabagh, Y.M. Moustafa, A. Hamdy, H.M. Killa, R.T.M. Ghanem, R.E. Morsi, Preparation and characterization of sulfonated polystyrene/magnetite nanocomposites for organic dye adsorption, Egypt. J. Pet., (2017).
[58] M. Tanzifi, K. Karimipour, M. Najafifard, S. Mirchenari, Removal of congo red anionic dye from aqueous solution using polyaniline/TiO_2 and polypyr role/TiO_2 nanocomposites: isotherm, kinetic, and thermodynamic studies. IJE Trans. C: Aspects, 29 (2016) 1659–1669.
[59] T. Hao, X. Rao, Z. Li, C. Niu, J. Wang, X. Su, Synthesis of magnetic separable iron oxide/carbon nanocomposites for efficient adsorptive removal of Congo Red, J. Alloy Compd., 617 (2014) 76–80.

[60] X. Yang, Z. Wang, M. Jing, R. Liu, L. Jin, X. Shen, Efficient removal of dyes from aqueous solution by meso porous nanocomposite $Al_2O_3/Ni_{0.5}Zn_{0.5}Fe_2O_4$ microfibers, Water Air Soil Pollut., 225 (2014) 1819.
[61] O. Paşka, R. Ianoş, C. Păcurariu, A. Brădeanu, Magnetic nanopowder as effective adsorbent for the removal of congo red from aqueous solution. Water Sci. Technol., 69 (2014) 1234–1240.
[62] L. Wang, A. Wang, Adsorption characteristics of congo red onto the chitosan/montmorillonite nanocomposite, J. Hazard Mater., 147 (2007) 979–985.
[63] M. Ghaemi, G. Absalan, L. Sheikhian, Adsorption characteristics of titan yellow and congo red on $CoFe_2O_4$ magnetic nanoparticles, J. Iranian Chem. Soc., 11 (2014) 1759–1766.
[64] K. Parashar, N. Ballav, N. Debnath, K. Pillay, A. Maity, Rapid and efficient removal of fluoride ions from aqueous solution using a polypyrrole coated hydrous tin oxide nanocomposite. J. Colloid. Interface. Sci., 476 (2016) 103–118.
[65] M.I. Khan, S. Akhtar, S. Zafar, A. Shaheen, M.A. Khan, R. Luque, A. ur Rehman, Removal of congo red from aqueous solution by anion exchange membrane (EBTAC) adsorption kinetics and thermodynamics, Materials., 8 (2015) 4147–4161.
[66] D. Hu, P. Wang, J. Li, L. Wang, Functionalization of micro crystalline cellulose with N, N-dimethyldodecylamine for the removal of congo red dye from aqueous solution, Bioresour., 9 (2014) 5951–5962.
[67] R. Mudzielwana, M.W. Gitari, T.A.M. Msagati, Characterisation of smectite-rich clay soil: implication for groundwater defluoridation, South Afri. J. Sci., 112 (2016) 1–8.
[68] H. Wang, Y. Shen, C. Shen, Y. Wen, H. Li, Enhanced adsorption of dye on magnetic Fe_3O_4 via HCl-assisted sonication pretreatment, Desalination, 284 (2012) 122–127.
[69] M. Bhaumik, R. McCrindle, A. Maity, Efficient removal of Congo Red from aqueous solutions by adsorption onto interconnected polypyrrole–polyaniline nano fibers, Chem. Eng. J., 228 (2013) 506–515.

Supporting information

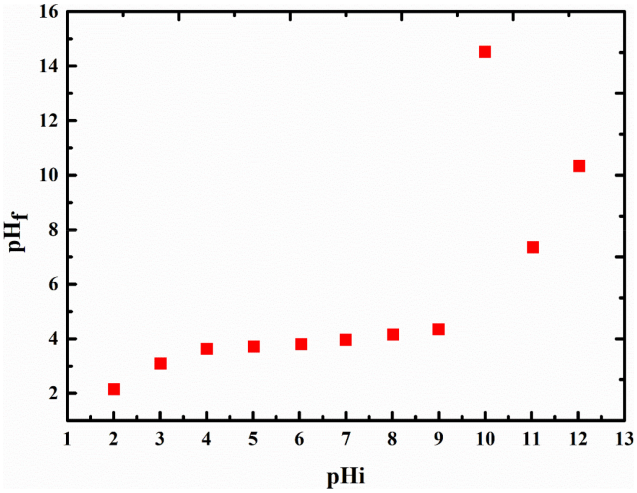

Fig. S1. Point of zero charge of PPy/Fe_3O_4 nanocomposite.

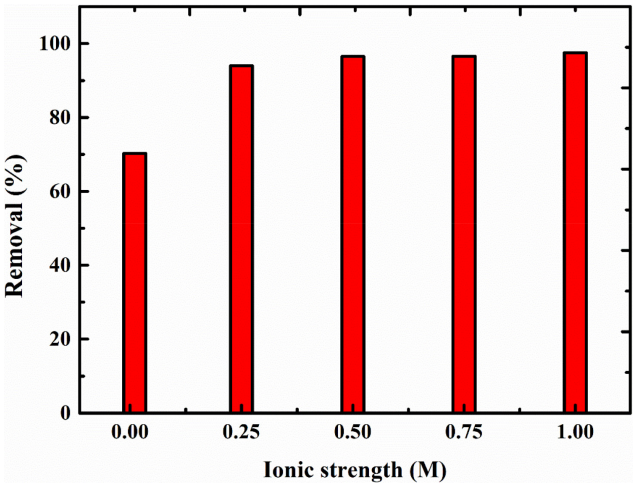

Fig. S2. Effect of ionic strength on the adsorption of CR by polypyrrole magnetic nanocomposite under the influence of magnetic field.

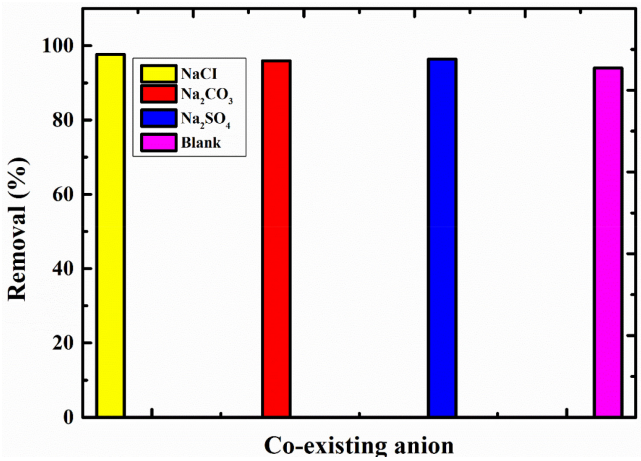

Fig. S3. Effect of co-existing anions on the adsorption of CR by polypyrrole magnetic nanocomposite under the influence of magnetic field.